Macromolecular Materials and Engineering, Volume 304, Issue 6, June 2019, Article number 0900033
DOI:10.1002/mame.201900033

Proanthocyanidins-induced horizontal arrangement poly(vinyl alcohol)/graphene composites with enhanced mechanical properties

Chao Wang, Min Wen, Le Guo, Boyu Zhang, Tingzhen Ming, Fuzhi Huang and Qi Zhang**

Chao Wang, Min Wen, Le Guo, Prof. Qi Zhang
School of Materials Science and Engineering, Wuhan University of Technology, 122 Luoshi Road, Wuhan 430070, China

Boyu Zhang
School of Physics and Electronics, Hubei University of Arts and Science, 296 Longzhong Road, Xiangyang 441053, China

Prof. Tingzhen Ming
School of Civil Engineering and Architecture, Wuhan University of Technology, 122 Luoshi Road, Wuhan 430070, China

Prof. Fuzhi Huang
State Key Laboratory of Advanced Technology for Materials Synthesis and Processing, Wuhan University of Technology, 122 Luoshi Road, Wuhan 430070, China
E-mail: Fuzhi.huang@whut.edu.cn (Fuzhi Huang)

Dr. Qi Zhang
School of Aerospace, Transport and Manufacturing, Cranfield University, Cranfield, Bedfordshire, MK43 0AL, UK
E-mail: Q.Zhang@cranfield.ac.uk (Qi Zhang)

Abstract

A green approach is employed to prepare mechanically-enhanced composites by adding non-covalently proanthocyanidins (PC)-modified graphene (PC-rGO) into poly(vinyl alcohol) (PVA). Ascorbic acid (AA) is used as the reducing agent and PC is used as a dispersant to synthesize low-defect and fully dispersed graphene. After static treatment, the PC-rGO sheets in the composite form a horizontally arranged structure. Compared with neat PVA, the Young's modulus of the graphene-modified composites is significantly enhanced by 79.3% with incorporation of 0.9 wt% PC-rGO. The composites incorporated with GO or AA-rGO (without PC) have randomly distributed GO structures and apparent rGO agglomeration, resulting in a weaker mechanical property. The dispersibility, degree of defects, distribution state of graphene, and interactions with the polymer matrix are directly related to the final mechanical performance. This new approach for mechanical enhancement of the graphene-embedded PVA composites provides the possibility for large-scale production of graphene-reinforced composite materials.

Keywords: nanocomposites; mechanical properties; green method; noncovalent functionalization graphene; self-assembly

1. Introduction

Graphene has been regarded as a rising star in material science since its discovery in 2004,[1] due to its excellent properties, such as huge specific surface area,[2] extremely high charge mobility,[3] great thermal conductivity,[4] and high Young's modulus.[5] Among them, the excellent mechanical properties make it be a good choice for nanofillers. Recently, graphene and its derivatives including graphene oxide (GO) and functionalized graphene oxide (FGO), are widely studied as composite nanofillers.[6] The key points, determining the final mechanical properties in the polymer/graphene systems, are high-quality graphene, excellent interface compatibility and horizontal arrangement, which means higher mechanical strength of graphene and more efficient transferring of the interfacial stress between graphene and polymer matrix.[7] Therefore, the choice of nanofillers becomes especially important.

In regard to mechanical properties, GO is inferior to graphene due to oxygen-containing functional groups on the surface and will form defect sites when subjected to external forces.[5a, 8] It can be speculated that nanofillers with stronger intrinsic properties exhibit better mechanical properties.[9] For instance, Liang et al., for the first time, prepared poly(vinyl alcohol) (PVA)/GO composites and revealed a 76 % improvement of tensile strength and a

62 % increase in Young's modulus at a low concentration of 0.7 wt% graphene oxide.[10] Meanwhile, Zhao et al. prepared PVA/rGO composites by directly heating the mixture of hydrazine hydrate, GO and PVA. An obvious 150 % improvement of tensile strength and an astonishing nearly 10 times increase of Young's modulus is achieved by incorporation of 1 wt% graphene.[11] In addition, fewer oxygen-containing functional groups in rGO in comparison with GO mean weaker interlayer hydrogen bonding.[12] It is for this reason that commonly used strong reducing agents would induce irreversible agglomeration of graphene occurring through strong π-π stacking and Van der Waals' interactions.[13] In order to avoid agglomeration of graphene sheets and promote good interactions between graphene and polymer matrix, FGO have been widely developed. Dispersible graphene sheets are usually prepared via chemical modification[9, 14] or non-covalent functionalization[7a, 15]. In contrast, non-covalent functionalization is identified to have less damage to the structure and properties of graphene.[16] Moreover, non-covalently modified graphene possesses free functional groups derived from adsorbed molecules, which can interact with the polymer substrate. The type and quantity of those functional groups directly determine the compatibility of graphene with the polymer. Wang et al. demonstrated the fabrication of poly(sodium 4-styrenesulfonate) (PSS)-coated PVA/rGO composites. An improvement of 48 % in tensile strength was obtained by adding only 0.3 wt% rGO, and a maximum increase of 55 % in the Young's modulus was achieved by adding barely 0.1 wt% rGO.[7b] Some attempts have been taken to prepare non-covalently modified graphene. Those chemical agents have been used as dispersants, such as poly-o-phenylenediamine (PoPD),[17] Poly(amic acid),[18] pyrene-terminated molecule (Py-LC),[19] polyethylene[20] and phosphorus–nitrogen compound.[21] Among them, the toxic characteristic of these chemical agents prevents the application of modified graphene in certain fields such as biomaterials, biosensors and food packaging. To solve this problem, green modifiers including pyrene derivative,[16c] tea polyphenol,[22] gallic acid[16a] and dopamine[23] have been used. Nevertheless, a part of the modifier is involved in the reduction of GO, while the redundant part acts as the stabilizer. Since the modifiers usually do not have high reduction ability, the low degree of reduction cannot maximize the enhancement of graphene/composite mechanical performance. Accordingly, the development of a green method for preparing high quality graphene nanofillers by combining strong reductant and dispersant will add a significant practical value for applications.[24]

In this study, a green method was adopted to modify graphene via non-covalent treatment. Proanthocyanidins (PC), which can be easily extracted from the skin and seed of Paiś grapes (Vitisvinifera L.), was chosen as stabilizer.[25] There are four separate branched chains,

one benzene ring on each branched chain and two hydroxyl groups on each benzene ring. This structure is similar to that of borate ions, which can promote the formation of layered structures.[26] Meanwhile, ascorbic acid (AA), which has a similar reducing power as hydrazine hydrate, was selected as a green reducing agent.[27] PVA was chose as the polymer matrix because of its excellent properties, including biodegradability, recyclability, and alternative.[10] The reaction mechanism of PC-rGO was discussed and the mechanical properties of the PVA/PC-rGO composites were tested. Attributed to the interaction bonding of PC molecules, it was found that after 6 h static treatment, PC-rGO sheets in the composites spontaneously formed a horizontal arrangement structure, even when they were dried at 50 ℃. (**Scheme 1**) However, there was no horizontal distribution in graphene oxide composites, suggesting that PC molecules promoted the process of self-assembly. Different from the traditional layer-by-layer deposition assembly and vacuum filtration assembly to prepare layered films, graphene tends to be horizontally distributed under the driving forces of solvent evaporation and gravity.[28] This way of self-assembly is simple and less energy consumption. Correspondingly, the mechanical properties of PVA/PC-rGO composites also showed higher improvements. Benefiting from excellent dispersibility and interfacial compatibility, as well as the regular horizontal arrangement of graphene sheets, the tensile strength and Young's modulus of the polymer are significantly improved.[18, 29] So far, this is the first discovery that PC molecules can induce the formation of the layered graphene composite. Without common vacuum filtration and layer-by-layer assembly processes and toxic chemicals, this method is feasibly promising for industrial large-scale production.

2. Experimental Section

2.1. Materials

Graphite powders of 325 mesh were purchased from Nanjing XFNANO Materials Tech Co., Ltd. Proanthocyanidins (PC, 98 %) was purchased from Shanghai Macklin Biochemical Co., Ltd. P_2O_5, $K_2S_2O_8$ and PVA1788 were purchased from Aladdin Chemical Co., Ltd. Ascorbic acid (AA), potassium permanganate ($KMnO_4$), sulfuric acid (H_2SO_4, 98 %), hydrogen peroxide (H_2O_2, 30 %), and hydrochloric acid (HCl) were purchased from Sinopharm Chemical Reagent Co., Ltd. All reagents used here were of analytical grade and used without further purification. The water used in this work was deionized water (resistivity > 18.25 MΩ·cm).

2.2 Preparation of graphene oxide

The GO sheets were prepared from purified natural graphite by a modified Hummers method.[30] Briefly, concentrated H_2SO_4 (40 mL) was added into a 150 mL flask filled with graphite (5 g), followed by the addition of $K_2S_2O_8$ (5 g) and P_2O_5 (5 g) was gradually added with stirring. The mixture was stirred at 80 ℃ for 4.5 h. The resultant blue dark mixture was cooled to room temperature, then diluted, filtered and washed with distilled water till the pH became neutral, and then the solid was dried at 40 ℃ under vacuum for 2 days. We named it pretreated graphite (P-G). H_2SO_4 (40 mL) was added to a three-necked flask and stirred in an ice bath. To this flask, P-G powder (1 g) and $KMnO_4$ (5 g) were gradually added into the above solution under controlled temperature of 10 ℃. Then stirring was continued for 2 hours. The temperature of the entire ice bath process was controlled below 10 ℃. The mixture was then stirred at 35 ℃ for 2 hours in an oil bath. The resulting solution was diluted by adding the deionized water (90 mL) under vigorous stirring for 1 hour, under controlled temperature less than 90 ℃. The obtained brick-red suspension was further diluted by adding extra deionized water (90 mL). H_2O_2 solution (10 mL, 30 %) was then added drop-wise with constantly stirring. The mixture became bright yellow. The resulting GO suspension was washed by repeated centrifugation, first with 10 % aqueous HCl solution to remove excess of manganese salt followed by deionized water until the pH of the solution became neutral. The suspension was successively centrifuged at 3000 and 10,000 rpm for 30 min to remove thick multilayer flakes and small pieces, respectively. Finally, the product was dried in vacuum.

2.3 Synthesis of PC-modified reduced graphene oxide

The sample was prepared according to the flow chart as shown in Scheme 1. Firstly, GO (100 mg) was added to the deionized water (100 mL) and exfoliated by ultrasonication for 30 min. After being completely dispersed, the suspension turned yellow brown and became homogeneously transparent. Then, PC (100 mg) was added to the GO dispersion and stirred at room temperature. After 2 h, AA (100 mg) was added to the above suspension. The mixture was then stirred at 90 ℃ for another 6 hours. Finally, the obtained dispersion was subjected to dialysis for a week to completely remove excess PC and reaction residues. The obtained dispersion was directly used after the concentration was calibrated, which was designated as PC-rGO. For comparison, the reduced graphene oxide (rGO) was synthesized by adding 100 mg of AA to GO dispersion (1 mg mL^{-1}) with continuous stirring and heating at 90 ℃ for 6 h. The same method was used to remove impurities. This sample was named as AA-rGO.

2.4 Preparation of PVA/PC-rGO composite films

A range of PC-rGO dispersions with known concentrations were prepared. Then PVA was added to each of these PC-rGO dispersion, stirring at 90 ℃ for 2 hours until completely dissolved. The obtained dispersion was degassed in an ultrasonic bath for 30 min. Then, the dispersion was poured into a petri dish and dried in an oven at 50 ℃ until the mass was completely constant. Prior to this, the Petri dish was sealed and placed on a horizontal abutment for 12 h to ensure self-assembly was completed. Among them, the mass fraction of PC-rGO relative to PVA was 0 %, 0.3 %, 0.5 %, 0.7 % and 0.9 %, which were designated as PVA, PVA/0.3PC-rGO, PVA/0.5PC-rGO, PVA/0.7PC-rGO and PVA/0.9PC-rGO, respectively. PVA/GO composites were prepared through the exactly same procedure, including PVA/0.3GO, PVA/0.5GO, PVA/0.7GO and PVA/0.9GO. At the same time, the PVA film containing 0.9 % AA-rGO was prepared by the same procedure as a reference, which was named PVA/AA-rGO.

2.5 Characterization

UV-vis absorption spectra were examined by a UV-vis-NIR spectrophotometer (Lambda 750S, PerkinElmer) in the spectral range of 800-200 nm with 1 nm step. FT-IR spectra characterizations were measured at ambient temperature by a FT-IR microscope and spectrometer (Nicolet 6700, Thermo Fisher). The spectral range was set to 500-4000 cm^{-1}. X-ray photoelectron spectra (XPS) were determined on an XSAM800 (Kratos Company, UK) with Al Kα radiation. Raman spectra (Renishaw-InVia) were carried out using a 514 nm laser to monitor the structural changes. X-ray diffraction patterns were examined by an X-ray Diffractometer (D8 advance, Bruker) provided Cu Kα radiation with λ = 1.5418 Å at 40 kV voltage and 40 mA current. Atomic force microscopy (AFM, Park NX10) was used to test the thickness of graphene with tapping-mode. The AFM samples were prepared by spin-coating the dispersed droplets (50 μL) on Si/SiO_2 wafers surface at 3000 rpm for 20 seconds. Field emission scanning electron microscopy (FESEM, Hitachi S-4800) was used to observe the cross section of composite films. Pre-place samples in a vacuum environment to remove the adsorbed water vapor, then slide out a notch with a surgical blade, quickly tear the film along the small nick. Thermogravimetric analysis tests were conducted in TGA Q50 (TA, USA). The tests started at room temperature and heated to 800 ℃ at a heating rate of 10 ℃ min^{-1} under N_2 atmosphere. Tensile tests were performed by MTS systems (China) Co., Ltd. at room temperature (60 % RH) with a cross-head speed of 2 mm min^{-1}. The tensile samples were made

into dumbbell-shaped according to ASTM D638, and five specimens for each sample were tested to obtain average and standard deviation values.

3. Results and discussion

3.1 Characterization of graphene-based nanofillers

The reduction process was detected by UV-vis absorption spectroscopy. In the digital images (**Figure 1**a), there were two groups: 1. GO: AA=1:1 wt% and 2. GO: PC: AA=1:1:1 wt%. The color gradually turned black from yellow brown. After the reaction was carried out for 40 min, significant agglomerated particles appeared in Group 1 (the red square part of Figure 1a). In contrast, the dispersion was still stable in Group 2 after 6 hours. At regular intervals, a portion of the dispersion was extracted from the reaction mixture for analysis. In order to avoid the influence of reaction residues, the suspension was washed with dilute hydrochloric acid solution and deionized water for several times. The spectra of Figure 1b corresponded to the dispersions of Group 2 at different times. GO dispersion showed a strong absorption peak at around 230 nm, which corresponded to the π-π* transition.[31] With the reaction time prolonged, the absorption peak gradually red-shifted and the absorbance in the whole visible range increased evidently, signifying the restoration of conjugated structure of graphene.[32] This transform corresponded to the change in the color of the dispersion. After an hour, the peak red-shifted to 268 nm, and then it remained unchanged over time. Consequently, the completion time of reaction was determined as an hour. In **Figure S1**, PC could not effectively disperse the graphene. These changes confirmed that PC and AA could work together to obtain a well-dispersed graphene dispersion with high degree of reduction.

FT-IR was investigated to detect the changing of oxygen-containing groups. In Figure 1c, the GO characteristic peaks correspond to various functional groups, including C–OH (alkoxy) stretching vibration peak at 1060 cm^{-1}, C–O (epoxy) stretching peak at 1226 cm^{-1}, O–H at 1412 and 3395 cm^{-1}, aromatic C=C stretching vibration at 1622 cm^{-1} and C=O stretching vibration peak (in both ketone and carboxylic acid groups) at 1733 cm^{-1}.[25] After reduced via AA, the absorption intensities of ketone and carboxylic acid groups (1720 cm^{-1}), O–H groups (3395 and 1410 cm^{-1}) and alkoxy groups (1052 cm^{-1}) decreased remarkably, which was similar to the previous literature.[33] After adding extra PC to the reaction, the intensity of absorption peaks correlated to the oxygen containing groups also decreased dramatically. Compared with that of AA-rGO, the C=O stretching vibration peak showed a similar degree of reduction. The absorption at the peak of epoxy groups exhibited a more significant reduction, which indicated that the epoxy groups were removed more thoroughly and that PC-rGO showed a higher degree

of reduction than AA-rGO. Conversely, in the range of 3300-3500 cm^{-1}, the IR absorption of PC-rGO slightly increased, indicating that the hydroxyl content of rGO was slightly increased. To explain this phenomenon, PC molecules were also detected, whose spectrum exhibited a strong hydroxyl characteristic peak, ascribing to PC molecules adsorbed onto graphene sheets by π-π interactions. This result was achieved probably because the PC molecules as dispersant restrained agglomeration, allowing more in-plane groups to be exposed and the reduction proceeds more thoroughly.[27]

To further determine the structural changes of functionalized graphene, XPS was performed to characterize the GO and rGO. As shown in Figure 1d, there were four distinguishable carbon-containing functional groups, which were located at 284.6 (C=C/C-C), 286.8 (C–O), 287.4 (C=O) and 289.0 eV (O–C=O).[34] In Figure 1e and 1f, those peak intensity of the C–O groups dramatically decreased after reaction, implying the effective reduction of GO. Meanwhile, the C/O ratio of GO was 2.13. After reduction, the C/O ratio of PC-rGO (3.33) presented a slightly higher than that of AA-rGO (3.16), suggesting that PC-rGO showed a slightly higher degree of reduction. As indicated in the FT-IR spectra (Figure 1c), the removal effect of the PC-rGO and AA-rGO on carbonyls is similar. PC-rGO displayed evidently less residue of epoxy groups and a slight increase in hydroxyl groups. In a previous report, a rGO stabilizer also made it exhibit a relatively lower C/O.[16a] If the hydroxyls introduced by the adsorption of PC molecules were removed, the C/O ratio of the actual graphene sheets would be higher. In other words, graphene received a higher degree of reduction after adding PC. This observation was in good agreement with the UV-vis and the FT-IR results.

The Raman spectra of GO and rGO were shown in **Figure 2**a. Two fundamental vibrations were observed at 1580 cm^{-1} and 1357 cm^{-1}, which were attributed to the G band and D band, respectively. The peak intensity ratio of the D band to the G band was used to estimate the ratio of the number of sp^2 carbon atoms to that of sp^3 carbon atoms.[35] It provides a strong evidence for the change in the electronic structure of graphene.[36] The D/G intensity ratio of AA-rGO was 1.46, which was higher than that of GO (1.29). The removal of hydroxyls and epoxy groups corresponded to the reduction of in-plane and edge defects. Simultaneously, the edge defects increased ascribed to the cracking of graphene sheets.[18] Unexpectedly, the D/G intensity ratio of PC-rGO (1.15) was even less than that of GO. This might be due to PC molecules adsorbed to the surface of graphene sheets, and the in-plane shear stress was balanced around the reduction process, which ultimately inhibited the cracking of graphene sheets.

It was natural to think that the adsorption of PC molecules might increase the interlayer spacing, which was confirmed by X-ray diffraction measurement (Figure 2b). As expected, GO

exhibited a relatively sharp diffraction peak at 9.8° with an interlayer spacing of 0.902 nm, in contrast to the peak of the graphite, that was more intense and thinner at 26.6° (d-spacing of 0.336 nm).[37] The inter-sheet distance was enhanced because of the insertion of water molecules and other oxygenated moieties generated by oxidation of graphite.[38] Meanwhile, AA-rGO and PC-rGO showed no diffraction peak around 9.8°, declaring that the oxygen-containing functional groups were mostly removed. In addition, AA-rGO and PC-rGO showed a wide diffraction peak at about 23.6° (0.377 nm) and 23.2° (0.383 nm), respectively, which were ascribed to the reduction and restacking of graphene sheets.[39] We could find that the addition of PC did give rise to the layer spacing, which was due to the adsorption of PC molecules on the rGO surface. Similar findings had also been found on tannin functionalized graphene.[40] The PC molecules were coated on the surface of graphene through π-π stacking, while hydroxyl groups of PC molecules formed hydrogen bonds between the graphene layers, increasing the interlamellar spacing.

The thickness of the samples was measured and characterized using atomic force microscope. In **Figure 3**a, the average thickness of GO was tested to be about 1.08 nm, which was similar to the previous literature.[16a] It was confirmed that GO sheets were single layers. In Figure 3c, AA-rGO presented a multi-layer stacking structure, which was consistent with the previous conclusions (Figure 1a). Meanwhile, Figure 3b showed that the average thickness of PC-rGO was about 2.57 nm. Referred to the previous literature, the thickness of the single-layer graphene sheets should be about 1.0 nm.[41] The thickness would apparently be increased due to adsorption of molecules.[42] Combining previous tests (Figure 1), it was absolutely determined that graphene was highly reduced. The increase in thickness of PC-rGO confirmed that the PC molecules were indeed adsorbed to the surface of graphene sheets. From another perspective, this result also confirmed the reason for the increase of interlayer spacing in X-ray diffraction (Figure 2b). To further verify their morphology, similar results were found using FESEM to detect the corresponding AFM samples (Figure S2, Supporting Information).

3.2 Characterization of PVA/PC-rGO composite films

Figure 4 showed the FESEM images for the cross sections of the composite films. Compared with the smooth surface of pure PVA, an apparent layered structure appeared after adding the PC-rGO, which implied that a self-assembly of PC-rGO and PVA in the film happened and the PC-rGO has excellent interactions with PVA.[18, 29] The nanostructure of the hybrid films clearly indicated the graphene layers.[7b] Although only 0.3 wt% PC-rGO was added, a small amount of discontinuous horizontal distribution could be observed in **Figure S3**c. As the content of PC-

rGO increased, a more pronounced horizontal distribution of the fault structure can be recognized. Between the layers, the notches and sheet-like protruding structures could be clearly observed, which was arranged in a state of uniform horizontal distribution. However, in some areas of PVA/AA-rGO, agglomerated graphene clusters could be easily distinguished, and other parts were similar to pure PVA. In order to compare the cross-sectional morphology, PVA/GO composite samples were prepared through the same preparation method. This phenomenon proved that PC-rGO could be well dispersed in the PVA and spontaneously form layered structure.[24, 29] The driving force of self-assembly came from the bridge-grafting effect of PC molecules. The benzene rings in the PC molecules adsorbed graphene sheets surface via the π-π bonds, and its hydroxyls form hydrogen bonds with the PVA matrix. Graphene tends to be horizontally distributed under the driving forces of solvent evaporation and gravity, and the viscosity of the corresponding dispersion becomes the resistance.[28a, 43] As shown in Figure S3e, the composite of PVA/0.9PC-rGO without the static treatment exhibited a chaotic distribution. Perhaps due to the difference in viscosity, PC-rGO needed to overcome less resistance than GO under the force of gravity and solvent evaporation.[44]

FT-IR had also been used to explore the changes of functional groups in composite membranes.[7b] As shown in **Figure 5**a, the wide and strong band at around 3451 cm^{-1} shifted to a lower wave number with the loading of PC-rGO increasing. This band was corresponded to the free and H-bonded hydroxyls.[31a] In addition to the shift of hydroxyl band, no new peak was observed, indicating that PC did not react with PVA. The shift of the hydroxyl band could be attributed to the formation of hydrogen bonds between the nanofillers and the hydroxyls of the PVA molecules, reducing the amount of hydrogen bonds between the PVA molecules.[9] The higher the weight fraction of PC-rGO, the larger the offset value of the hydroxyl bond. Compared with PVA/0.9PC-rGO (3427 cm^{-1}), PVA/AA-rGO had the same weight ratio of nanofillers, but the peak position was 3440 cm^{-1}, indicating that good dispersion facilitated hydrogen bonds formation. This result was consistent with the variation of the layered structure in the FESEM (Figure 4). Furthermore, this phenomenon could demonstrate that the hydrogen bonding between layers promoted the horizontal arrangement of graphene sheets.

XRD was also utilized to investigate the degree of crystallization of the polymer. Figure 5b and **Figure S4** illustrated the XRD patterns of neat PVA and its nanocomposite films. There were no characteristic peaks of GO and PC-rGO in the XRD patterns of composites, which implied that both GO and PC-rGO were well dispersed in the PVA matrix.[26, 28a] However, AA-rGO/PVA did not show the characteristic peak of AA-rGO, probably because the amount of graphene added was not enough.[11] The broadened peak at about 19.3° indicated the existence

of an amorphous structure.[45] It was noticed that incorporation of less than 0.5 wt% PC-rGO only slightly increases the intensity of the unique characteristic peak of composite films. As the amount of PC-rGO added increased, the intensity of the peak at about 19.3° gradually increased. A similar phenomenon also could be found in many polymer/graphene nanocomposites and was considered to be a result of polymer crystallization that was induced by graphene.[46] Since the fully exfoliated and well-dispersed graphene nanosheets act as nucleating agents, the crystallinity of the composites will be improved, corresponding to the intensity of the characteristic peak.[11] In contrast, PVA/0.9PC-rGO exhibited more pronounced enhancement of the characteristic peak than PVA/0.9GO and PVA/AA-rGO, implying that the adding of graphene sheets promoted crystallization of PVA and uniform dispersion was the guarantee of higher crystallinity. This result was consistent with the images shown in the FESEM (Figure 4).

TGA was further employed to characterize the thermal properties of PVA and its nanocomposites. **Figure 6**a showed the trend of weight with temperature increasing. PVA degraded at a relatively higher temperature than those nanocomposites. Furthermore, the temperature of the maximum degradation rate was determined by differential thermogravimetric analysis (DTA) results (Figure 6b). The peak temperature (T_p) of the DTG curve represented the temperature at which the maximum weight loss rate was reached. The T_p of PVA/PC-rGO showed a decreasing trend as the amount of nanofillers added increased, indicating that decomposition occurred at lower temperatures.[47] In contrast, the T_p of PVA/AA-rGO was just slightly reduced. These phenomena were attributed to uniform distribution and outstanding thermal conductivity of graphene, accelerating the decomposition rate of the PVA.

Figure 7a, b exhibited the typical tensile stress-strain curves of the PVA, PVA/PC-rGO and PVA/GO composite films. Figures 7c-7d showed the corresponding Young's modulus and tensile strength as the changes of nanofillers' amount (specific values are presented in **Table S1**). With the increase of nanofillers, the modulus of the PVA/PC-rGO composites increased gradually, from 2.66 GPa for neat PVA to a maximum value of 4.77 GPa for the PVA/0.9PC-rGO nanocomposites (an increase of 79.3 %). Meanwhile, the tensile strength of PVA/PC-rGO nanocomposites increased sharply by 75.2 % to 103.0 MPa with the addition of 0.7 wt% PC-rGO, and then decreased slightly with further increase in PC-rGO content. Even just 0.3 wt% PC-rGO could significantly improve the mechanical properties. In contrast to PVA/PC-rGO composites, the tensile strength increased by 42.5 % to 83.8 MPa and the Young's modulus increased by 48.9 % to 3.96 GPa with the concentration of 0.7 wt% GO. Those composites with GO showed a relatively lower improvement, ascribing to the random disorder of GO sheets.

Due to the horizontal arrangement of graphene sheets and strong hydrogen bonding, tensile stress would be effectively transferred onto graphene sheets.[48] Whereas, after the nanofillers were added in excess, the distance between PC-rGO sheets became smaller and the interactions between PC-rGO sheets became stronger, which made rGO sheets tend to distribute obliquely and even vertically.[7b, 29] Thus, the mechanical properties of PVA/0.9PC-rGO appeared to decrease. In addition, the test of PVA/AA-rGO can be found in **Figure S5**. As expected, PVA/AA-rGO exhibited a very limited improvement in mechanical properties. Therefore, to enhance mechanical properties as much as possible, the ordered horizontal alignment and intrinsic excellent properties of graphene are critical.

4. Conclusion

Highly dispersible non-covalently modified graphene was prepared using natural substances, PC (dispersant) and AA (reducing agent). This method eventually obtains a high-quality graphene sheet with more excellent dispersibility, lower defectivity and higher degree of reduction relative to the use of AA alone. In the process of compounding with PVA, PC molecules act as the critical bridges in the formation of layered structures. Specifically, the aromatic rings of PC and graphene sheets form π-π interactions, and its hydroxyl groups form hydrogen bonds with the hydroxyl groups inside the PVA molecules. The mechanical properties of the PVA/PC-rGO composites showed a significant enhancement, with a 75.2 % improvement of tensile strength in the incorporation of 0.7 wt% PC-rGO and a 79.3 % increase of Young's modulus in its incorporation of 0.9 wt%. Through the comparison of the properties obtained from various samples, dispersion and interfacial interactions was considered to act as the indispensable roles in mechanical properties of polymer/graphene system. Ultimately, it is worth noting that the addition of PC molecules induces the production of horizontal structures, which suggests a new route for the preparation of graphene layered materials with high mechanical performance. The entire process of self-assembly is spontaneously performed under intermolecular interactions, which makes large-scale production possible.

Supporting Information

Supporting Information is available from the Wiley Online Library or from the author.

Acknowledgements

This study is financially supported by the Hubei Provincial Natural Science Foundation of China [grant numbers 2018CFA029].

References

[1] K. S. Novoselov, A. K. Geim, S. V. Morozov, D. Jiang, Y. Zhang, S. V. Dubonos, I. V. Grigorieva, A. A. Firsov, *Science* **2004**, *306*, 666-669.

[2] J. Wang, C. Wu, Q. Deng, K. Jiang, L. Shang, Z. Hu, J. Chu, *Nanoscale* **2018**, *10*, 13140-13148.

[3] T. Soltani, A. Tayyebi, B.-K. Lee, *Sol. Energy Mater. Sol. Cells* **2018**, *185*, 325-332.

[4] H. Malekpour, K. H. Chang, J. C. Chen, C. Y. Lu, D. L. Nika, K. S. Novoselov, A. A. Balandin, *Nano Lett.* **2014**, *14*, 5155-5161.

[5] a) L. Liu, J. Zhang, J. Zhao, F. Liu, *Nanoscale* **2012**, *4*, 5910-5916; b) Y. Gao, P. Hao, *Phys. E* **2009**, *41*, 1561-1566.

[6] a) J. Li, Y. Song, Z. Ma, N. Li, S. Niu, Y. Li, *Ultrason. Sonochem.* **2018**, *43*, 1-8; b) R. Surudzic, A. Jankovic, M. Mitric, I. Matic, Z. D. Juranic, L. Zivkovic, V. Miskovic-Stankovic, K. Y. Rhee, S. J. Park, D. Hui, *J. Ind. Eng. Chem.* **2016**, *34*, 250-257; c) Z. Ismail, A. H. Abdullah, A. S. Zainal Abidin, K. Yusoh, *Appl. Nanosci.* **2017**, *7*, 317-324.

[7] a) H. Bai, Y. Xu, L. Zhao, C. Li, G. Shi, *Chem. Commun.* **2009**, *151*, 1667-1669; b) X. Wang, X. Liu, H. Yuan, H. Liu, C. Liu, T. Li, C. Yan, X. Yan, C. Shen, Z. Guo, *Mater. Des.* **2018**, *139*, 372-379.

[8] a) X. Tang, C. Mu, W. Zhu, X. Yan, X. Hu, J. Yang, *Carbon* **2016**, *98*, 432-440; b) Y. Zhu, S. Murali, W. Cai, X. Li, J. W. Suk, J. R. Potts, R. S. Ruoff, *Adv. Mater.* **2010**, *22*, 5226.

[9] L. Shao, J. Li, Y. Guang, Y. Zhang, H. Zhang, X. Che, Y. Wang, *Mater. Des.* **2016**, *99*, 235-242.

[10] J. Liang, Y. Huang, L. Zhang, Y. Wang, Y. Ma, T. Guo, Y. Chen, *Adv. Funct. Mater.* **2009**, *19*, 2297-2302.

[11] X. Zhao, Q.-H. Zhang, D.-J. Chen, P. Lu, *Macromolecules* **2011**, *44*, 2392.

[12] L. Shao, J. Li, Y. Zhang, S. Gong, H. Zhang, Y. Wang, *J. Mater. Chem. A* **2014**, *2*, 14173-14180.

[13] a) C. Bao, Y. Guo, L. Song, Y. Hu, *J. Mater. Chem.* **2011**, *21*, 13942-13950; b) S. Stankovich, R. D. Piner, X. Chen, N. Wu, S. T. Nguyen, R. S. Ruoff, *J. Mater. Chem.* **2006**, *16*, 155-158.

[14] a) R. Wissert, P. Steurer, S. Schopp, R. Thomann, R. Mülhaupt, *Macromol. Mater. Eng.* **2010**, *295*, 1107-1115; b) M. Soheilmoghaddam, H. Adelnia, H. C. Bidsorkhi, G. Sharifzadeh, M. U. Wahit, N. I. Akos, A. A. Yussuf, *Macromol. Mater. Eng.* **2017**, *302*, 1600260.

[15] S. Das, F. Irin, H. S. Tanvir Ahmed, A. B. Cortinas, A. S. Wajid, D. Parviz, A. F. Jankowski, M. Kato, M. J. Green, *Polymer* **2012**, *53*, 2485-2494.

[16] a) J. Li, G. Xiao, C. Chen, R. Li, D. Yan, *J. Mater. Chem. A* **2013**, *1*, 1481-1487; b) Z. Yu, Z. Shi, H. Xu, X. Ma, M. Tian, J. Yin, *Carbon* **2017**, *114*, 649-660; c) Y. Xu, H. Bai, G. Lu, C. Li, G. Shi, *J. Am. Chem. Soc.* **2008**, *130*, 5856-5857.

[17] S. Qin, M. Cui, Z. Dai, S. Qiu, H. Zhao, L. Wang, A. Zhang, *Tribol. Lett.* **2018**, *66*, 1-10.

[18] G. Y. Kim, M.-C. Choi, D. Lee, C.-S. Ha, *Macromol. Mater. Eng.* **2012**, *297*, 303-311.

[19] Z. Tong, W. Zhuo, J. Zhou, R. Huang, G. Jiang, *J. Mater. Sci.* **2017**, *52*, 10567-10580.

[20] A. A. Vasileiou, M. Kontopoulou, A. Docoslis, *ACS Appl. Mater. Interfaces* **2014**, *6*, 1916-1925.

[21] W. Chen, P. Liu, L. Min, Y. Zhou, Y. Liu, Q. Wang, W. Duan, *Nano-Micro Lett.* **2018**, *10*, 39.

[22] Q. Huang, L. Hao, J. Xie, T. Gong, J. Liao, Y. Lin, *ACS Appl. Mater. Interfaces* **2015**, *7*, 20893-20901.

[23] W. Lee, J. U. Lee, B. M. Jung, J.-H. Byun, J.-W. Yi, S.-B. Lee, B.-S. Kim, *Carbon* **2013**, *65*, 296-304.

[24] J. Guo, L. Ren, R. Wang, C. Zhang, Y. Yang, T. Liu, *Composites, Part B* **2011**, *42*, 2130-2135.

[25] C. Mellado, T. Figueroa, R. Baez, R. Castillo, M. Melendrez, B. Schulz, K. Fernandez, *ACS Appl. Mater. Interfaces* **2018**, *10*, 7717-7729.

[26] N. Yan, F. Capezzuto, M. Lavorgna, G. G. Buonocore, F. Tescione, H. Xia, L. Ambrosio, *Nanoscale* **2016**, *8*, 10783-10791.

[27] J. Zhang, H. Yang, G. Shen, P. Cheng, J. Zhang, S. Guo, *Chem. Commun.* **2010**, *46*, 1112-1114.

[28] a) R. K. Layek, K. R. Ramakrishnan, E. Sarlin, O. Orell, M. Kanerva, J. Vuorinen, M. Honkanen, *J. Mater. Chem. A* **2018**, *6*, 13203-13214; b) H. Liu, T. Kuila, N. H. Kim, B.-C. Ku, J. H. Lee, *J. Mater. Chem. A* **2013**, *1*, 3739-3746; c) Y.-Q. Li, T. Yu, T.-Y. Yang, L.-X. Zheng, K. Liao, *Adv. Mater.* **2012**, *24*, 3426-3431.

[29] X. Yang, Y. Tu, L. Li, S. Shang, X.-m. Tao, *ACS Appl. Mater. Interfaces* **2010**, *2*, 1707-1713.

[30] W. S. Hummers, Jr., R. E. Offeman, *J. Am. Chem. Soc.* **1958**, *80*, 1339.

[31] a) Y. Tan, Y. Song, Q. Zheng, *Nanoscale* **2012**, *4*, 6997-7005; b) N. H. Kim, T. Kuila, J. H. Lee, *J. Mater. Chem. A* **2013**, *1*, 1349-1358.

[32] D. Li, M. B. Mueller, S. Gilje, R. B. Kaner, G. G. Wallace, *Nat. Nanotechnol.* **2008**, *3*, 101-105.

[33] K. K. H. De Silva, H.-H. Huang, M. Yoshimura, *Appl. Surf. Sci.* **2018**, *447*, 338-346.

[34] O. Sadak, A. K. Sundramoorthy, S. Gunasekaran, *Carbon* **2018**, *138*, 108-117.

[35] A. C. Ferrari, J. Robertson, *Philos. Trans. R. Soc., A* **2004**, *362*, 2477-2512.

[36] C. A. Johnson, K. M. Thomas, *Fuel* **1984**, *63*, 1073-1080.

[37] S. Bose, T. Kuila, A. K. Mishra, N. H. Kim, J. H. Lee, *J. Mater. Chem.* **2012**, *22*, 9696-9703.

[38] S. Ganguly, P. Das, P. P. Maity, S. Mondal, S. Ghosh, S. Dhara, N. C. Das, *J Phys. Chem. B* **2018**.

[39] I. K. Moon, J. Lee, R. S. Ruoff, H. Lee, *Nat. Commun.* **2010**, *1*, 73.

[40] K. H. Thebo, X. Qian, Q. Zhang, L. Chen, H.-M. Cheng, W. Ren, *Nat. Commun.* **2018**, *9*, 1-8.

[41] C. Zhu, S. Guo, Y. Fang, S. Dong, *ACS Nano* **2010**, *4*, 2429-2437.

[42] S. Roy, X. Tang, T. Das, L. Zhang, Y. Li, S. Ting, X. Hu, C. Y. Yue, *ACS Appl. Mater. Interfaces* **2015**, *7*, 3142-3151.

[43] S. Pourhashem, M. R. Vaezi, A. Rashidi, M. R. Bagherzadeh, *Corros. Sci.* **2017**, *115*, 78-92.

[44] D. Li, Y. Liu, H. Ma, Y. Wang, L. Wang, Z. Xie, *RSC Adv.* **2015**, *5*, 31670-31676.

[45] S. Shang, L. Gan, C. W. M. Yuen, S.-x. Jiang, N. M. Luo, *Composites, Part A* **2015**, *68*, 149-154.

[46] J. Chen, Y. Gao, W. Liu, X. Shi, L. Li, Z. Wang, Y. Zhang, X. Guo, G. Liu, W. Li, B. D. Beake, *Carbon* **2015**, *94*, 845-855.

[47] L. Zhang, Y. Li, H. Wang, Y. Qiao, J. Chen, S. Cao, *Chem. Eng. J.* **2015**, *264*, 538-546.

[48] B. Liang, H. Zhao, Q. Zhang, Y. Fan, Y. Yue, P. Yin, L. Guo, *ACS Appl. Mater. Interfaces* **2016**, *8*, 28816-28823.

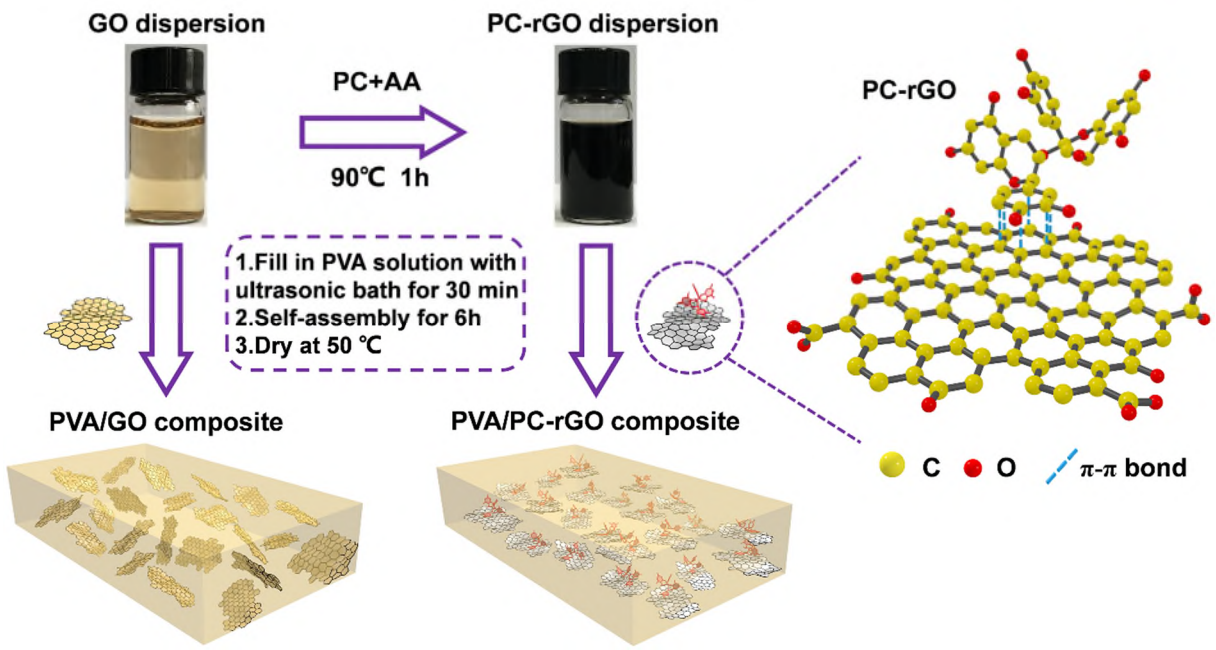

Scheme 1. A probable mechanism of fabrication of layered structure PVA/PC-rGO composites.

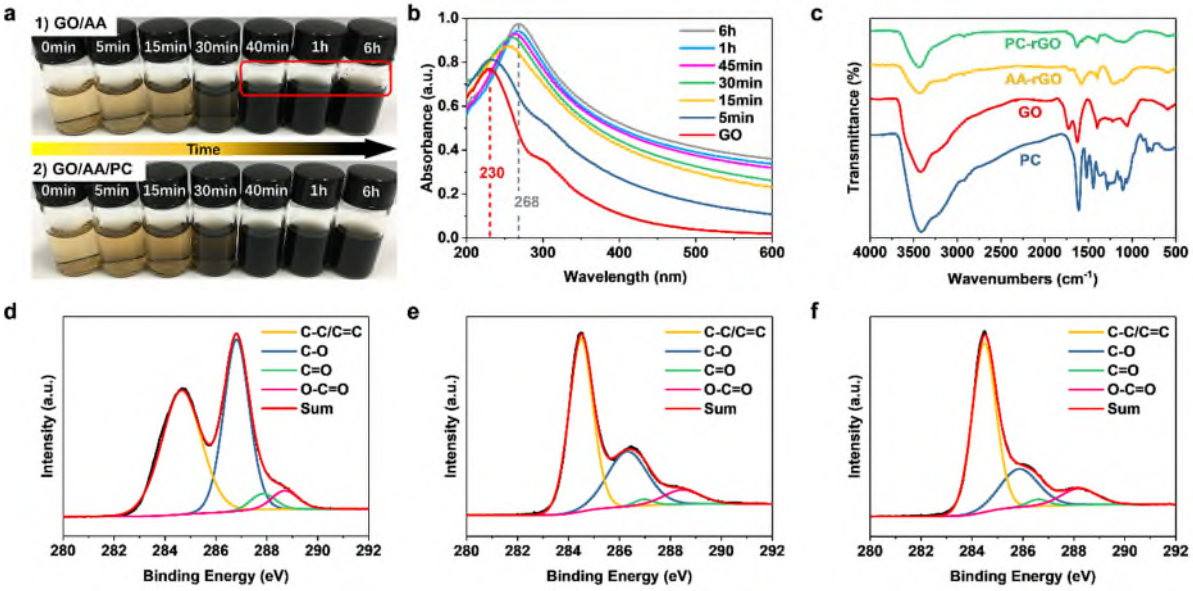

Figure 1. Characterization of GO, AA-rGO and PC-rGO. (a) Digital images, (b) UV-vis spectra, (c) FT-IR spectra, and (d, e, f) XPS spectrum (C1s) of the GO, AA-rGO and PC-rGO, respectively.

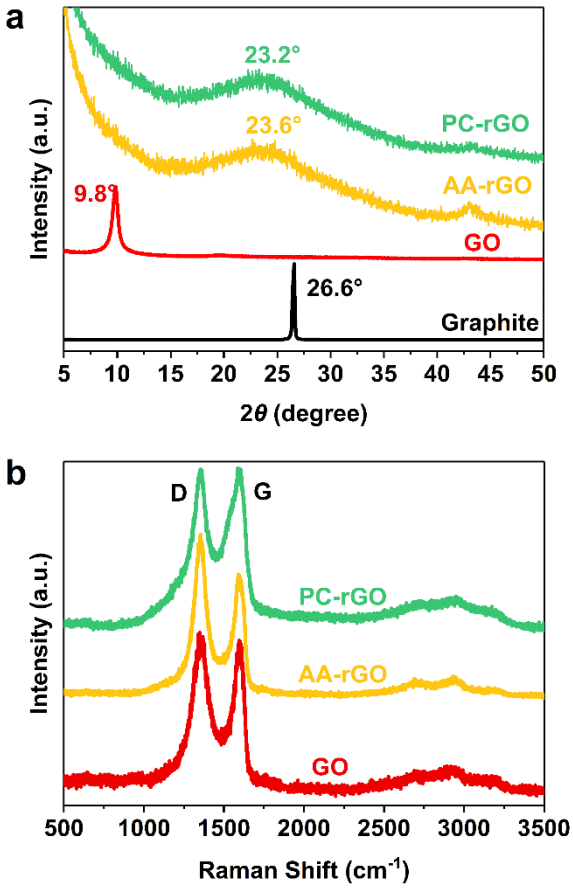

Figure 2. (a) XRD patterns of graphite, GO, AA-rGO and PC-rGO, and (b) Raman spectra of GO, AA-rGO and PC-rGO.

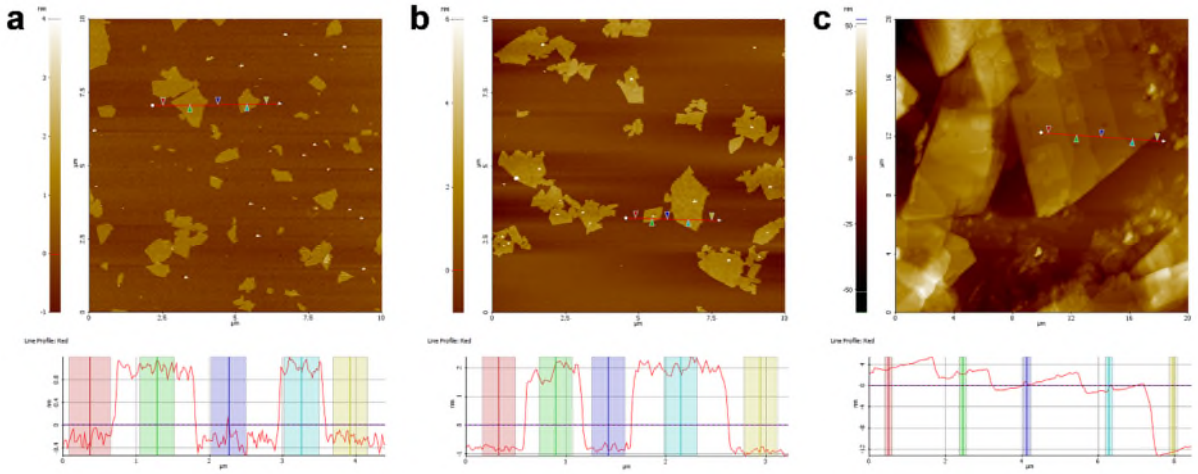

Figure 3. AFM images of (a) GO, (b) PC-rGO, and (c) AA-rGO deposited on Si/SiO_2 wafers surface.

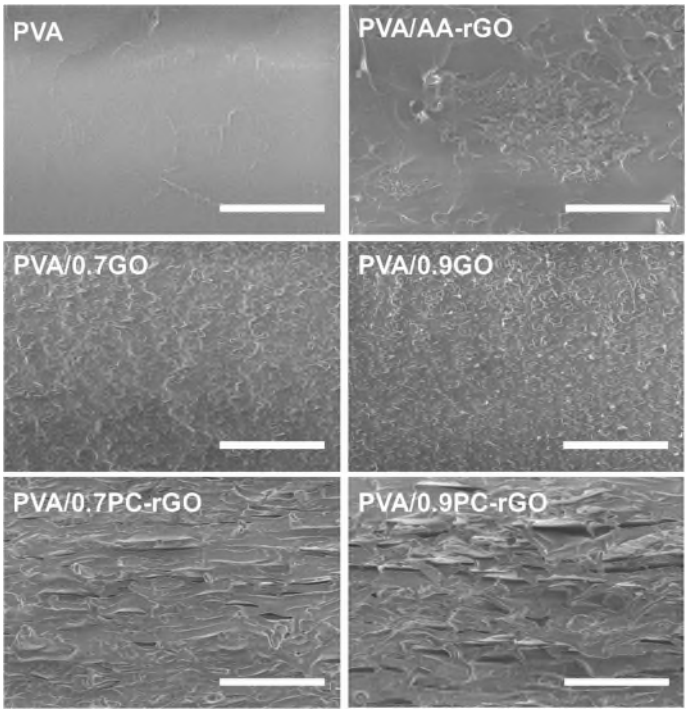

Figure 4. FESEM images of cross-section. (The scale rod represents 10 μm for all the images.)

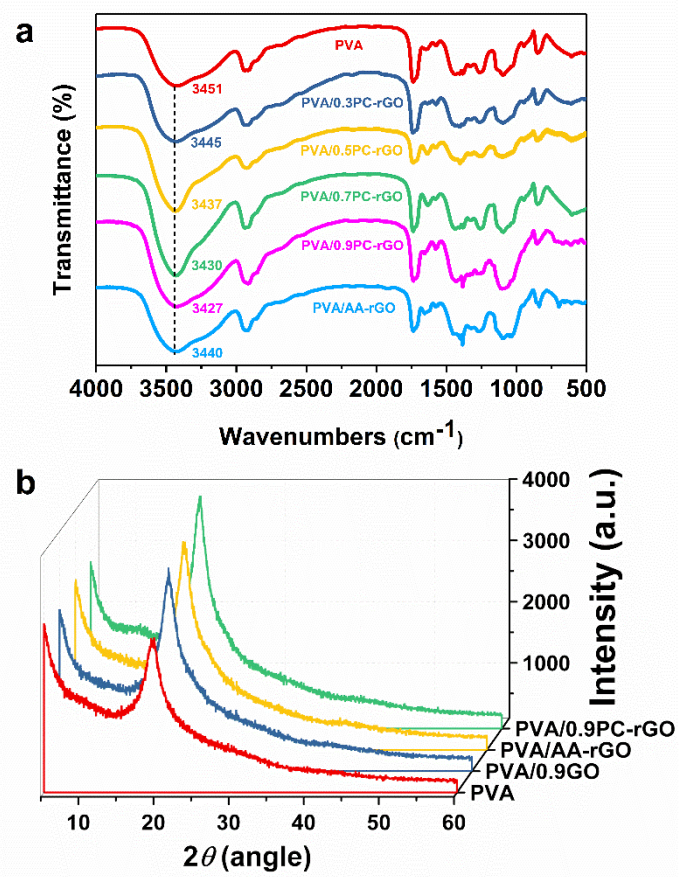

Figure 5. (a) FT-IR spectra of composite films, and (b) XRD patterns of PVA, PVA/0.9GO, PVA/AA-rGO and PVA/0.9PC-rGO composite films.

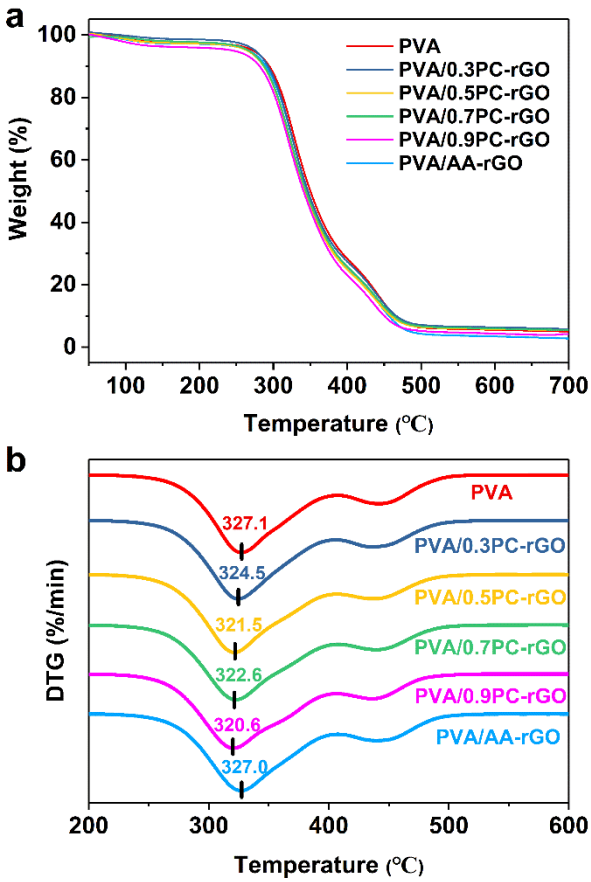

Figure 6. (a) TGA curves of the samples of PVA, PVA/PC-rGO and PVA/AA-rGO composite films, and (b) DTG curves of those samples obtained by calculating the first derivative.

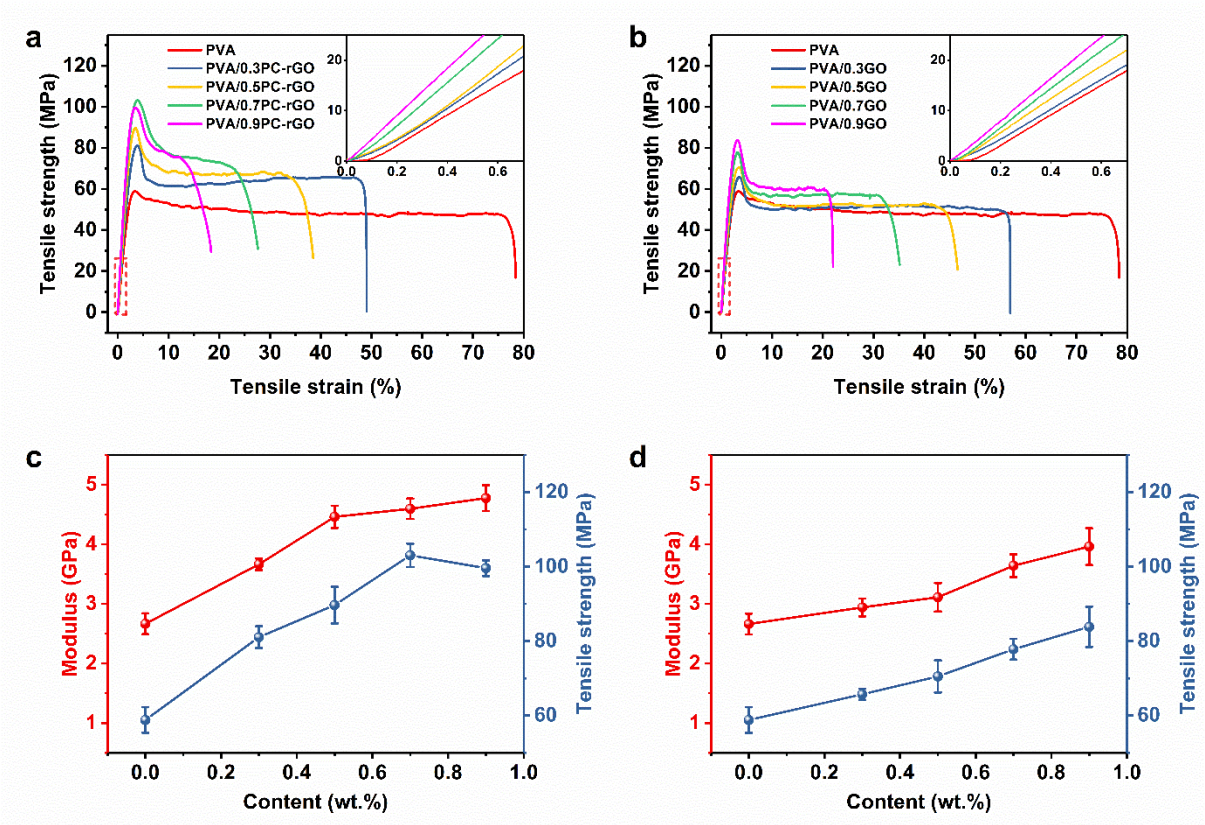

Figure 7. (a, b) Representative stress–strain curves for neat PVA and PVA/PC-rGO, as well as PVA/GO and (c, d) the variations of Young's modulus and tensile corresponding to different content of PC-rGO and GO.

Layered structure of graphene/poly(vinyl alcohol) mechanically reinforced film is prepared by proanthocyanidins grafting. As a nanofiller, graphene oxide is randomly distributed. Attributed to the grafting effect of proanthocyanidins at the interface, a layered distribution exhibits after modification, as well as mechanical properties increasing. This green synthesis method is promising for the large-scale production of horizontal arrangement mechanically reinforced graphene composites.

Keyword: nanocomposites

Chao Wang, Min Wen, Le Guo, Boyu Zhang, Tingzhen Ming, Fuzhi Huang* and Qi Zhang*

Proanthocyanidins-induced horizontal arrangement poly(vinyl alcohol)/graphene composites with enhanced mechanical properties

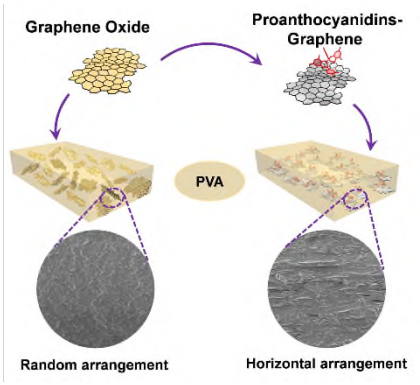

Supporting Information

Proanthocyanidins-induced horizontal arrangement poly(vinyl alcohol)/graphene composites with enhanced mechanical properties

Chao Wang, Min Wen, Le Guo, Boyu Zhang, Tingzhen Ming, Fuzhi Huang and Qi Zhang**

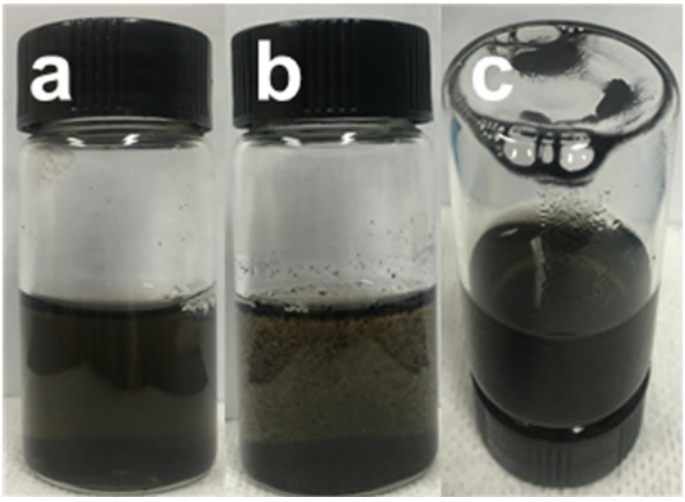

Figure S1. Digital images of (a) graphene dispersion dispersed by PC, (b) and (c) the dispersion after standing for 1 h.

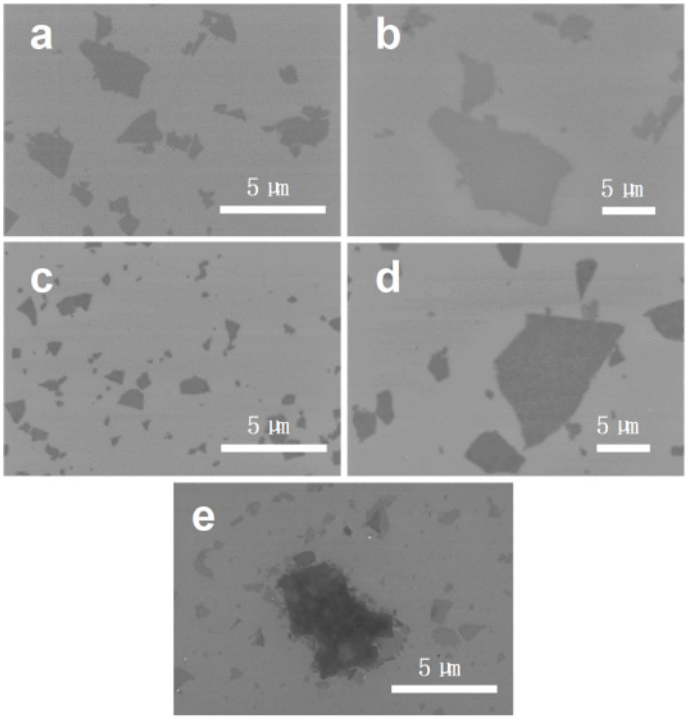

Figure S2. FESEM images of (a & b) GO, (c & d) PC-rGO and (e) AA-rGO deposited on Si/SiO_2 wafers surface.

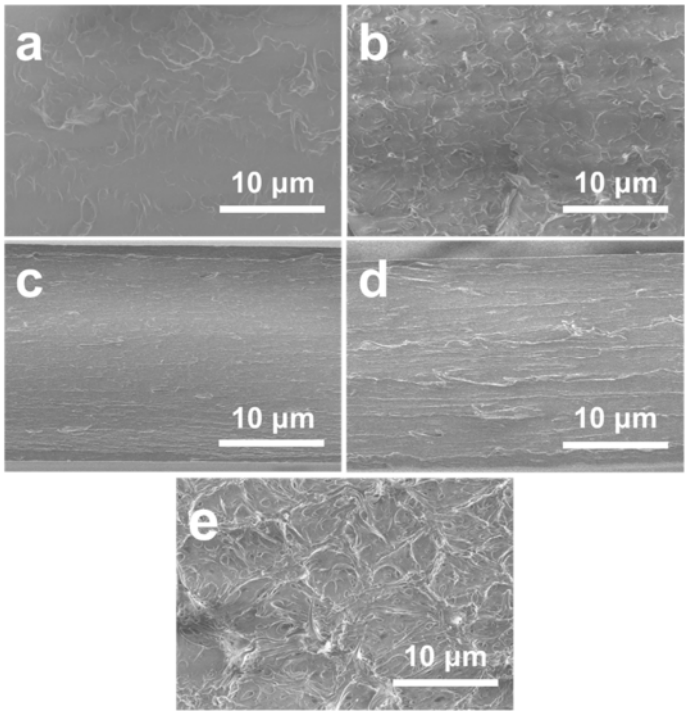

Figure S3. FESEM images of cross-section of (a) PVA/0.3GO, (b) PVA/0.5GO, (c) PVA/0.3PC-rGO, (b) PVA/0.5PC-rGO and (e) PVA/0.9PC-rGO (directly dried without 6 hours' static self-assembly).

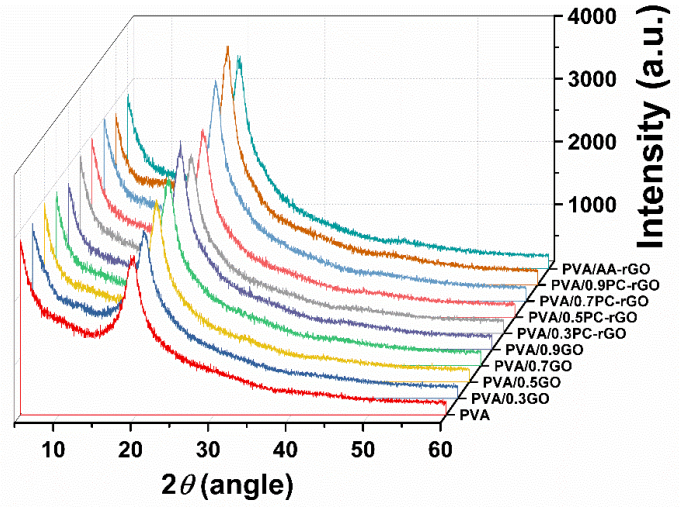

Figure S4. XRD patterns of composite films.

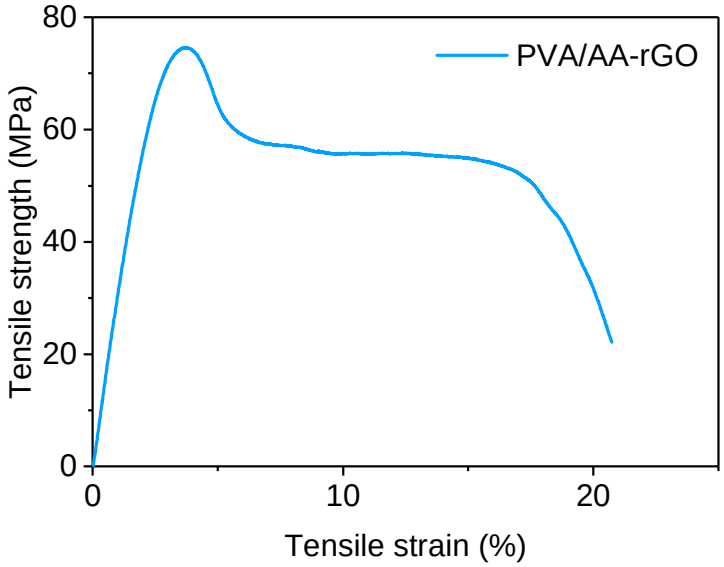

Figure S5. Representative stress–strain curves for PVA/AA-rGO.

Table S1. Mechanical property of neat PVA and its composite films.

Samples	Tensile strength (MPa)	Young's modulus (GPa)	Elongation (%)
PVA	58.8±3.5	2.66±0.18	78.4±2.9
PVA/0.3PC-rGO	81.0±2.9 (37.8 %)	3.66±0.10 (37.6 %)	49.1±3.4
PVA/0.5PC-rGO	89.7±4.9 (52.6 %)	4.46±0.19 (67.7 %)	38.5±2.9
PVA/0.7PC-rGO	103.0±3.1 (75.2 %)	4.59±0.17 (72.6 %)	27.6±5.2
PVA/0.9PC-rGO	99.6±2.1 (69.4 %)	4.77±0.22 (79.3 %)	18.4±3.1
PVA/0.3GO	65.7±1.5 (11.7 %)	2.96±0.15 (10.5 %)	56.9±4.6
PVA/0.5GO	70.5±4.3 (19.9 %)	3.11±0.24 (16.9 %)	46.6±6.3
PVA/0.7GO	77.8±2.8 (32.3 %)	3.64±0.19 (36.8 %)	35.2±2.7
PVA/0.9GO	83.8±5.4 (42.5 %)	3.96±0.31 (48.9 %)	22.0±4.2
PVA/AA-rGO	74.6±2.5 (26.9 %)	2.92±0.13 (9.8 %)	20.7±2.5

Note: Percentage values within parentheses are the relative change compared with PVA reference.